Hindawi
Australian Journal of Grape and Wine Research
Volume 2023, Article ID 7376153, 9 pages
https://doi.org/10.1155/2023/7376153

AUSTRALIAN SOCIETY OF VITICULTURE AND OENOLOGY | ASVO

Research Article

Evaluating the Potential of High-Resolution Visible Remote Sensing to Detect Shiraz Disease in Grapevines

Yeniu Mickey Wang[1,2] **Bertram Ostendorf**[3] **and Vinay Pagay**[1]

[1]*School of Agriculture, Food & Wine, Waite Research Institute, University of Adelaide, PMB 1, Glen Osmond, SA 5064, Australia*
[2]*CSIRO, Manufacturing, Autonomous Sensors Future Science Platform, 13 Kintore Ave, Adelaide, SA 5000, Australia*
[3]*School of Biological Sciences, The University of Adelaide, Molecular Life Sciences Building, North Terrace Campus, Adelaide, SA 5005, Australia*

Correspondence should be addressed to Vinay Pagay; vinay.pagay@adelaide.edu.au

Received 11 November 2022; Revised 8 December 2022; Accepted 20 March 2023; Published 5 May 2023

Academic Editor: K. J. Evans

Copyright © 2023 Yeniu Mickey Wang et al. This is an open access article distributed under the Creative Commons Attribution License, which permits unrestricted use, distribution, and reproduction in any medium, provided the original work is properly cited.

Background and Aims. Shiraz disease (SD) is a viral disease associated with *Grapevine virus A* that causes significant yield loss in economically important grape cultivars in Australia such as Shiraz and Merlot. Current diagnostic methods are time-consuming and costly. This study evaluates an alternative methodology using visible remote sensing imagery to detect SD in Shiraz grapevines. *Methods and Results*. High-resolution visible remote sensing images were captured of Shiraz grapevines in two South Australian viticultural regions over two seasons. The projected leaf area (PLA) of individual grapevines was estimated from the images. Virus-infected vines had significantly lower PLA than healthy vines in the early season but fewer difference after veraison. The lower PLA was only observed in grapevines coinfected with grapevine leafroll-associated viruses (GLRaVs) and Grapevine virus A (GVA). Shiraz vines infected with either GLRaVs or GVA had similar PLA to healthy vines. *Conclusions*. High-resolution RGB remote sensing technology has the potential to rapidly estimate SD infection in Shiraz grapevines. Our observations of shoot devigouration only in coinfected vines calls into question the etiology of SD. Further validation of the PLA technique incorporating different regions, seasons, cultivars, and combinations of viruses is needed for improving the robustness of the method. *Significance of the Study*. This preliminary study presents a new rapid and low-cost surveillance method to estimate SD infections in Shiraz vineyards, which could significantly lower the cost for growers who conduct on-ground SD visual assessments or lab-based tissue testing at the vineyard scale.

1. Introduction

Shiraz disease (SD) is a devastating viral disease of grapevines that was first reported on Merlot from South Africa [1]. SD disrupts the physiological development of grapevines and causes significant yield loss in specific cultivars, including Shiraz, Merlot, Malbec, and Sumoll [2]. The symptoms of SD infection in Shiraz include delayed budburst with restricted spring growth, lack of lignification on some canes, and delayed leaf senescence well into the dormant season [3, 4]. SD symptoms are latent (no symptoms) in tolerant cultivars such as Chardonnay and Cabernet Sauvignon; however, the viruses can be transmitted to susceptible cultivars (Shiraz and Melot) by mealybugs and soft scales [5, 6]. *Grapevine virus A* (GVA) group II variants were associated with SD [7, 8]. GVA also causes a rugose wood disease known as "Kober stem grooving" [9]. GVA often coexists with grapevine leafroll-associated viruses (GLRaVs) [6, 10–12], which is a group of viruses that causes Grapevine leaf disease (GLD) [13]. In Australia, GLRaV-1, GLRaV-3, and GLRaV-4 strain 9 (GLRaV-9) are commonly associated with GVA in SD-infected vines [14]. There are only a few effective methods to control grapevine viral diseases including roguing infected vines, replanting with certified, virus-free material, and controlling the vectors to stop the virus from spreading [15, 16]. It is therefore critical to accurately detect the patterns and extent of viral infections in vineyards to stop the virus from spreading further.

Standard detection methods for SD include serological methods, nucleic acid-based methods, and visual assessment [17, 18]. Lab-based methods are costly, thus limiting the number of grapevines tested and, consequently, an underestimation of the true incidence of virus infection in vineyards [17, 19]. Currently, the recommended minimum test rate by commercial diagnostic labs is five vines per thousand (0.5%) across the block [20]. Conducting on-ground visual assessments is labour-intensive, subjective, and sometimes unreliable. Low-altitude airborne remote sensing enables the capture of high detail with greater potential to rapidly survey the vineyards. Various optical sensors including red-green-blue (RGB), multispectral, hyperspectral, and thermal sensors have been used on the ground or platforms like unmanned aerial vehicles (UAVs) and manned fixed-wing aircraft for grapevine disease detection [21–26]. RGB imagery acquired through UAV-based remote sensing was used for the current study due to its relative simplicity compared to multi and hyperspectral images. A vertical projection of the canopy from the aerial image, the projected leaf area (PLA), for each vine was calculated from the image to compare the canopy size between healthy and SD-infected vines. PLA acquired from remote sensing imagery has a positive correlation to the canopy area. For example, Raj et al. [27] achieved an R^2 of 0.84 and RMSE of 0.36 by using PLA calculated from UAV RGB image and compared to leaf area index of maize.

In this study, we used high-resolution RGB remote sensing imagery to systematically assess PLA of individual healthy and diseased vines to predict SD infection in Shiraz grapevines in the field. The specific objectives of this study were: (1) to develop a simple remote sensing methodology that can consistently assess grapevine canopy size (using PLA as a surrogate) as a visual indicator of SD infection; (2) to confirm PLA-based disease status classification with lab-based tissue analysis; (3) to evaluate the time series of remote sensing imagery in order to conduct a spatial-within-season temporal analysis of canopy size differences between healthy and infected vines; and (4) to evaluate the temporal consistency of seasonal patterns of canopy development across multiple growing seasons. Our overarching goal was to develop a rapid and low-cost surveillance platform for SD detection at the vineyard scale.

2. Materials and Methods

2.1. Study Sites and Visual Estimation of Virus Infection. Two virus-infected Shiraz blocks (some vines previously tested positive with GVA and GLRaVs) were selected in different climatic wine regions in South Australia (SA) for this study. The first vineyard was in Monash, located in the warm inland region of Riverland (34°13′28″S, 140°33′01″E). A block of 1.5 ha of Shiraz was selected for the study. The soil type of vineyard was sand over limestone. The block was drip-irrigated with 7.5 ml·ha^{-1} of water per year. Approximate 50 kg ha^{-1} N and 50 kg·ha^{-1} P fertiliser were applied through fertigation annually. The vines were consistently machine spur pruned with a same size box shape each winter. Vineyard management was consistent between seasons. Integrated pest management was as per convention in this region, which generally has low disease pressure due to its warm-to-hot climate. The second vineyard was in the Barossa region, located in Lyndoch, SA (34°35′28″S, 138°53′01″E). A 1.5 ha block was chosen for the study. The soil type of the block was Calcic on red Sodosol. It was drip-irrigated with approximate 1 ml·ha^{-1} water per year. Both solid fertiliser and fertigation were applied at the rate of 130 kg·ha^{-1} N, 55 kg·ha^{-1} P, and 9 kg·ha^{-1} K annually. Shiraz was consistently two-bud spur pruned to 20 buds per m each winter. Details of the study sites (vineyards) are provided in Table 1.

2.2. Virus Testing. Laboratory-based tissue testing was used for ground-truthing (Figure 1(b)). Tissue samples were collected based on visual symptoms for virus testing, of which half the vines were symptomatic and half were asymptomatic. Leaf petioles were sampled near harvest time [28]. The leaves were carefully selected from the base of the shoots to avoid errors associated with sampling from a potential long shoot coming through from a neighbour vine. Four petioles near the base of the shoots (two from each side of the canopy) were sampled and transported with chilled ice packs.

All samples were virus-tested in the lab using an enzyme-linked immunosorbent assay (ELISA) [29]. The ELISA test kits produced by Bioreba (Reinach, Switzerland) were used to test GVA, GLRaV-1, GLRaV-3, and GLRaV-4 strains. 20% of these leaves samples were tested with reverse-transcription polymerase chain reaction (RT-PCR) [17, 30] for confirmation of the ELISA results. The RT-PCR test was conducted by a commercial diagnostics lab that routinely tests for grapevine viruses. Six commonly occurring grapevine viruses in Australia [31] were tested: GVA, GLRaV-1, GLRaV-3, GLRaV-4, GLRaV-4 strain 6, and GLRaV-4 strain 9. The result showed a 100% match between PCR and ELISA, confirming the reliability of the ELISA test. The number of vines in each class is shown in Table 2. Because GLRaV-1, -3, and -4 complexes cause similar GLD symptoms in grapevines, vines infected with either a single or combination of any GLRaVs were treated as a GLRaV infection. In total, there were four classes: (i) healthy, (ii) GVA only, (iii) GLRaVs only, and (iv) GVA + GLRaVs.

2.3. High-Resolution Remote Sensing: Data Collection and Processing. DJI Mavic 2 Pro (SZ DJI Technology Co., Ltd, Shenzhen, China) was used for image collection in this study (Figure 1(a)). The UAV uses a Hasselblad RGB camera with a 28 mm focal length and f/2.8–f/11 aperture. The field of view is approximate 77° and the image size is 5472 × 3648. Flight planning was automated by the Pix4D app (Pix4D S.A., Prilly, Switzerland) with the setting of nadir view, side and forward overlapping at approximate 80%, altitude at 45 m above ground level, and forward flight direction. The calculated spatial resolution of the images was approximate 1 cm pixel^{-1}.

Aerial image data were collected between October to April in S1 and September to April in S2. Data were captured at approximate monthly intervals (one flight per month) based on weather conditions (low wind and sunny) which resulted in six flights in Riverland and ten flights in Barossa (Table 1).

Table 1: Vineyard study sites used in the trial.

Vineyard locations	Planting year	Rootstock	Spacing (row × vine)	Vine density (vines ha^{-1})	Occurrence of symptoms (%)	Flight per season		Images per block
						S1	S2	
Riverland	1998	K51–40	3.5 × 3.5 m	816	5	6	8	288
Barossa	Grafted in 2015	Cabernet sauvignon	3.2 × 1.5 m	2165	15	10	8	290

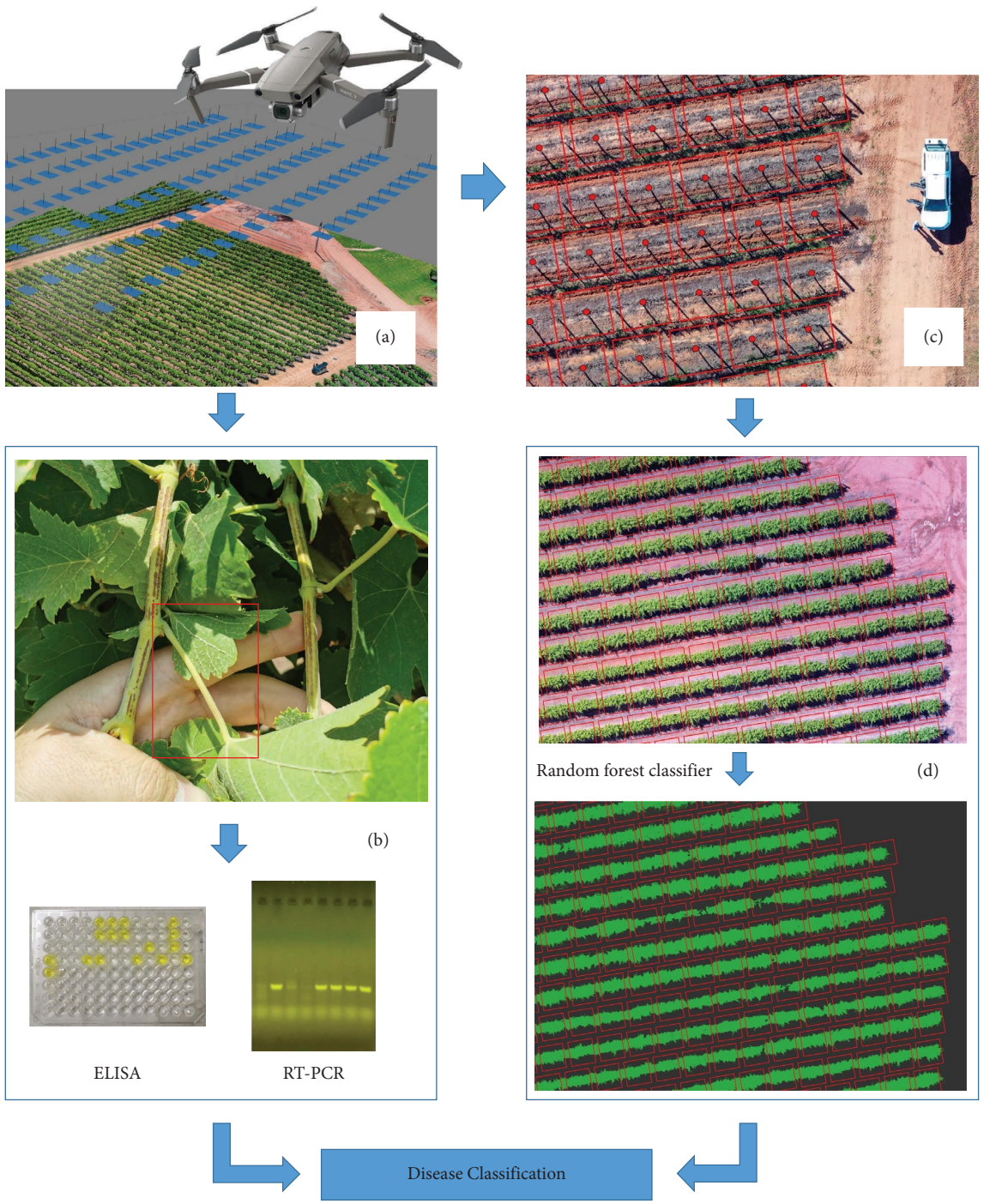

Figure 1: The workflow for disease classification with UAV images. (a) UAV data collection; (b) tissue sampling (petiole) and virus testing; (c) geo-locating and buffer creation for individual vines using the image at dormancy; and (d) grapevine canopy classification using random forest classifier.

All remote sensing imagery was captured under sunny and cloudless conditions between 11:00 to 15:00 h. In each flight, 288 images were taken for the Riverland block and 290 images for the Barossa block.

UAV Image mosaicking was conducted with Agisoft Metashape Professional, Version 1.6.2. (Agisoft LLC, St. Petersburg, Russia) to generate projected images with geo-information for each vineyard at each time point. Based on flight altitude and the resolution of the DJI Mavic 2 Pro camera, the mosaicked images produced a 1 cm pixel^{-1} ground sampling distance. The image geo-processing was conducted with ArcGIS Pro V2.8 (Esri, Redlands, California, US). Individual vines were geolocated using the image at dormancy when the shadow of vine trunks was clearly visible. Grapevine locations were manually digitised, and square buffers were created along with the orientation of row lines (Figure 1(c)). The size of the buffer was adjusted to about 90% of vine spacing to avoid the overlapping area

Table 2: The ELISA test results. Samples classified as "healthy" tested negative for GVA, GLRaV-1, -3, and -4; GVA only is grapevine virus A positive (single infection) but GLRaVs negative; GLRaVs only is single or any combination of grapevine leafroll-associated virus-1, -3, or -4 positive but GVA negative; GVA + GLRaVs is coinfection of both GVA and one or more GLRaV-1, -3 or -4.

	Healthy	GVA only	GLRaVs only	GVA + GLRaVs	Total
Riverland	23	3	0	16	42
Barossa	19	7	6	14	46

between vines. The vine spacing was larger in the Riverland Shiraz block (3.5 × 3.5 m vine and row spacing) compared to Barossa and Adelaide Hills vineyards (spacing 1.5 × 3.0 m), which results in a larger canopy therefore a larger buffer area per vine. Orthomosaics from each date were georeferenced to the dormancy image in order to accurately coalign vines.

The grapevine canopy was mapped using a supervised random forest classifier [32] (also called the random tree method in ArcGIS Pro). We used the ArcGIS Pro V2.8 random trees method with a maximum number of trees of 30 and a maximum tree depth of 15. Pixels in the image were classified as "Grapevine," "Soil," "Shadow," and Weeds." We manually labelled 5–7 training polygons in each training class and found the training data was sufficient to train Random Tree for classifying all pixels in the images. The "Soil," " Shadow," and "Weeds" classes were combined into a "non-grapevine" class to obtain a binary image for canopy area calculation (Figure 1(d)). To improve classification accuracy, different training data sets were created for early, middle, and later seasons as changing colour in the canopy over time. As undervine weeds were well controlled in all blocks, the grapevine was visually clearly distinguishable from the nongrapevine. The classification results were visually assessed by comparing the RGB and classified images, and results were consistent in all images, thus quantitative accuracy assessment of classification results was not required.

The projected leaf area (PLA) per individual vine was calculated as the sum of pixels that classified to "Grapevine" within square reference areas that were adapted to the vine and row spacing of the different vineyards. We used a square area of 3 × 3 m in Riverland, and 1.4 × 1.4 m in Barossa.

2.4. Statistical Analysis. Two-way ANOVA was used for statistical analysis using GraphPad Prism v9.0.0 (San Diego, CA, US). The PLA value of all virus-tested vines was used for analysis. Mean PLA values between each class (healthy, GVA only, GLRaVs only, and GVA + GLRaVs) at each time point were compared. Tukey's multiple comparisons test was used as a post hoc test ($p < 0.05$).

3. Results and Discussion

3.1. Symptoms of Shiraz Disease. The ground visual observations showed that SD-infected Shiraz vines had delayed budburst by approximate 15–20 days and smaller canopies in spring as indicated visually (Figure 2(a)). However, by midsummer (approximate fruitset stage), healthy and infected vines had indistinguishable canopies (Figure 2(b)). However, the canes of infected vines showed a lack of lignification, as shown in Figure 2(c). SD-infected vines were clearly identified in winter due to delayed leaf fall (delay approximate 15–20 days), which shows red leaves attached to the vine, while healthy vines had no leaves (Figure 2(d)). The SD symptoms consistently showed in two seasons and locations, this matched with observations in other studies [2, 4, 33].

3.2. PLA Difference between SD Symptomatic and Asymptomatic Canopy. The average PLA was calculated for each class (healthy, GVA only, GLRaVs only, and GVA + GLRaVs) in both blocks and seasons at each time point (Figure 3). In Riverland, the average size of coinfected (GVA + GLRaVs) vines was consistently approximate 1 m^2 smaller than healthy vines at 25 days after budburst (2.24 m^2 for healthy and 1.32 m^2 for coinfected vines) and flowering stage (4.42 m^2 for healthy and 3.62 m^2 for coinfected vines) in S1 (Figure 3(a)). The statistical analysis showed the GVA + GLRaVs classes were significantly ($p < 0.0001$) different from healthy in the early season. However, the difference in PLA between the two classes decreased after flowering. Figure 3(b) shows PLA of coinfected vines was approximate 1.3 m^2 smaller than healthy vines at 24 days after budburst (1.92 m^2 for healthy and 0.72 m^2 for coinfected vines) and flowering stage (4.26 m^2 for healthy and 2.82 m^2 for coinfected vines) in S2. Similar to S1, the difference in S2 between healthy and coinfected vines decreased after flowering; however, it still has a significant difference before veraison (with $p < 0.0001$).

In the Barossa vineyard, the PLA of coinfected Shiraz was also significantly smaller than that of healthy in the early season, especially at the flowering stage. In S1, the average PLA of the healthy and coinfected vines at the flowering stage was approximate 1.5 m^2 and 1.0 m^2 ($p < 0.0001$), respectively, thus coinfection resulted in 33% smaller PLA (Figure 3(c)). However, the difference between the two classes started to decrease at veraison and no significant differences were observed in PLA in the latter part of the growing season. The PLA difference between diseased and healthy vines was reduced by veraison although still significant ($p = 0.0307$). The p-values for the difference between healthy and coinfected vines were more significant around the flowering stage than at other times in both seasons.

The results indicated the symptomatic SD infection in Shiraz could be predicted using PLA calculated from RGB remote sensing images. The PLA of healthy and SD-infected vines had the highest difference between 20 and 70 days after bud burst, which unveils the optimum time window for SD detection as symptoms could be easily identified due to the significantly smaller PLA of the diseased vines. The PLA of SD-infected vines were 30%–70% smaller than the average healthy vines. We suggest setting a PLA threshold of 70% in healthy vines to classify as an SD infection in Shiraz. Therefore, PLA values at or less than 70% are classified as being SD infected. This threshold works between 15–45 days

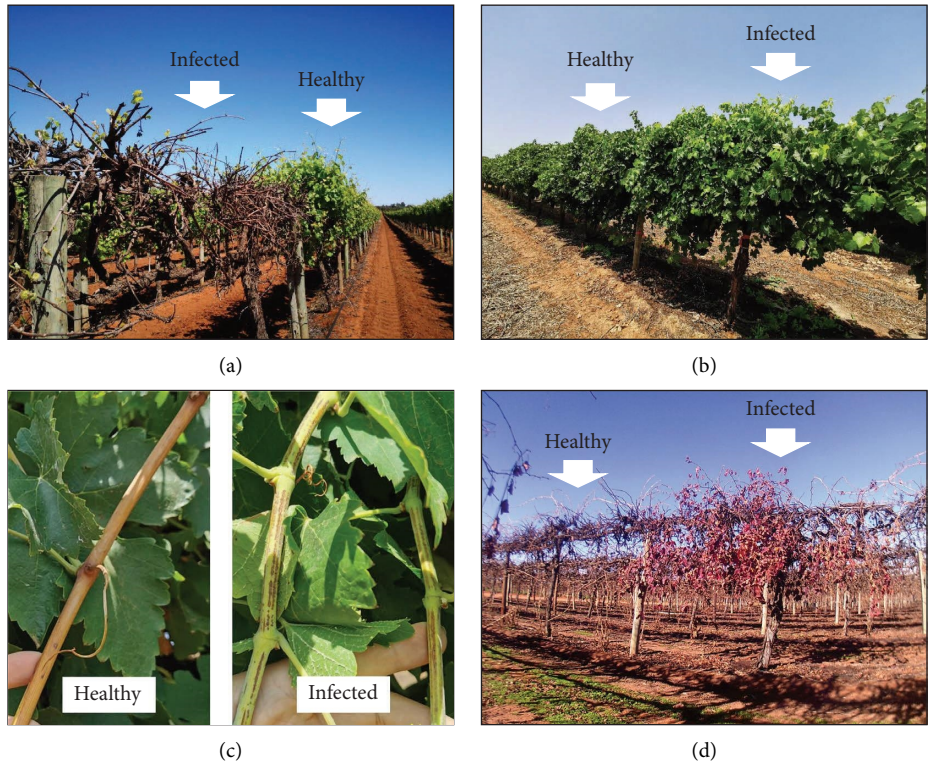

FIGURE 2: Symptoms of SD-infected Shiraz. (a) Restricted spring growth with delayed bud burst in Shiraz; (b) Shiraz canopies fully developed in midsummer at fruit set (EL-27); (c) canes of infected Shiraz show a lack of lignification at véraison (EL-35); and (d) red leaves remain on infected Shiraz vines while healthy vines drop all leaves during the dormant season.

after the budburst in the Riverland region and between 30–60 days after the budburst in the Barossa region. From veraison onwards, this method appeared to be less effective as canopy size differences between infected and healthy vines become smaller. However, our early PLA results could not distinguish SD from Grapevine trunk disease (GTD), a debilitating fungal disease that affects grapevines worldwide, causing devigourated shoots, and sometimes dead cordons [34]. The PLA of GTD-infected vines would likely remain low throughout the season since dieback results in very few growing shoots and death of the cordons [35, 36]. In contrast, SD-infected vines appear similar in growth to GTD-infected vines, but in contrast to GTD vines, have fully-developed canopies by the veraison stage; this key difference can be used to differentiate SD infection from GTD or dead vines. The PLA of SD-infected vines were 5%–15% smaller than the average healthy vines at this stage. Thus, we suggest that an 85% PLA threshold be used at the veraison stage to distinguish between SD-and GTD-infected or dead vines. Therefore, if the PLA is at or below 85% of the PLA of healthy vines between 90–120 days after budburst, the vine could possibly have GTD or be dead. Therefore, a minimum of two data collection timepoints are suggested per season, one in the early season and one in the mid-to-late season for determining SD using remote sensing. However, as the technique is an indirect detection method, which measures the canopy response to the virus, we cannot exclude the possibility that various other factors could be altering the phenotype. For example, other biotic stresses (fungal diseases), abiotic stresses (drought, salinity, heat stress, and mechanical damage), and virus strains and coinfections could influence vegetative growth and alter PLA [37]. Therefore, this remote sensing technique is indicative but not a conclusive method for SD infection. The current results were based on two study sites and years, the further assessments and virus testing validations are needed for the different regions, years, the age of vines, and cultivars. As additional information is acquired, different recommendations of the PLA threshold can be used for vineyards that have similar conditions.

If validated, this method can potentially be scaled to larger regions using RGB imaging from manned aircraft, or even satellite imagery in the future as their camera resolutions continue to increase.

3.3. Difference between Coinfection and Single Infections. Canopy development of coinfected vines (GVA + GLRaVs) lagged behind healthy vines due to delayed budburst in spring. This pattern was consistent in both vineyards and seasons (Figure 3). In comparison, the development of GVA and GLRaV (single infection) infected vines had no significant difference from healthy vines in both blocks or seasons. Despite previous studies showing that GVA and its variants are associated with SD [8], there is little systematic information between coinfection and SD symptoms. As the coinfection of GLRaVs and GVA is commonly found in vines, it is important to

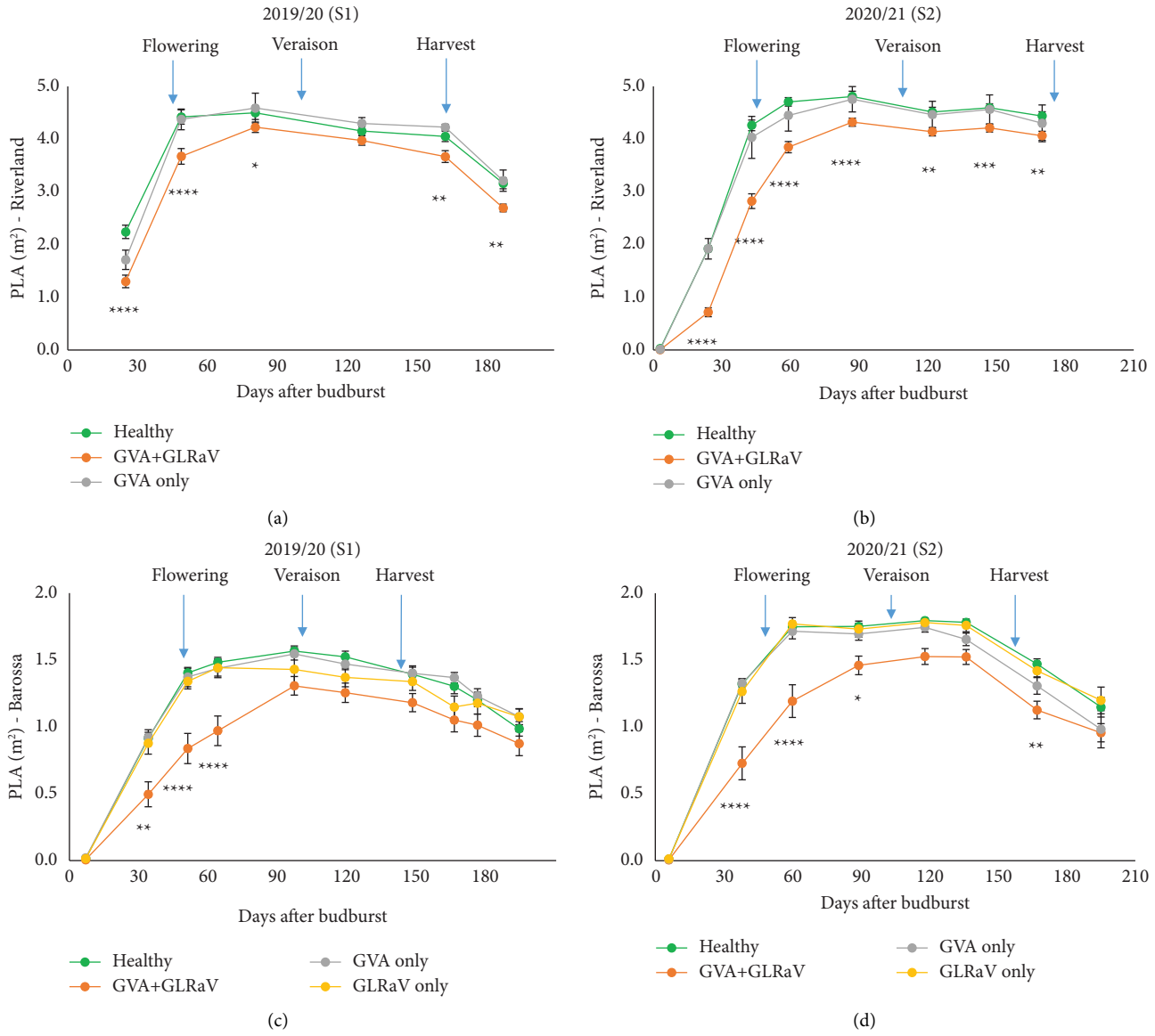

FIGURE 3: Average PLA for each lab-tested class at different times for both seasons in two vineyards. The p-value of healthy vs GVA + GLRaV shows in the graph, with $^{*}p \leq 0.05$, $^{**}p \leq 0.01$, $^{***}p \leq 0.001$, $^{****}p \leq 0.0001$, and nonsignificant with a blank. (a, b) Riverland Shiraz in S1 and S2; (c, d) Barossa Shiraz in S1 and S2.

consider both coinfection as well as environmental factors when studying disease symptoms.

The study found that SD symptoms in both Shiraz blocks only occur in vines that are coinfected with GVA and one or more GLRaVs, which in the vineyards we surveyed, were found to be mostly GLRaV-1 or GLRaV-4 strain 9 (GLRaV-9). We did not observe any typical SD symptoms when Shiraz vines were infected with GVA only (i.e., without GLRaVs). Similarly, Goszczynski and Habili [8] reported that SD symptoms in Shiraz were always associated with GVA group II and GLRaV-3 in South Africa. Consistent with the results of the present study, the same authors also observed that some vines did not exhibit any SD symptoms when infected with GVA group II alone; however, only visual evidence, but no quantitative evidence, was provided. GVA variants of group II have been closely associated with SD, but not groups I and III [3]. As the ELISA serological method is unable to discriminate between virus variants, the asymptomatic GVA-infected vines in our study could belong to group I and/or III. A previous study also reported that the variant GTR1-2 in GVA group II did not produce SD symptoms in Shiraz; however, other group II variants (BMO32-1, KWVMo4-1, and P163M5) produced SD symptoms in both Shiraz and Merlot [33]. The GVA variants in our study were unknown because the GVA primers used for the RT-PCR test in our study were not variant-specific. However, if the GVA variants in the present study did not belong to either group I or III, or the GTR1-2 variant (in group II), we could then infer that coinfection of GVA and GLRaVs is a requisite for SD symptoms in Shiraz. We are

unaware of any systematic studies that have been done to understand the relationship between SD symptoms and the combination of various viruses and their variants. This hypothesis requires a comprehensive investigation, potentially by using next-generation sequencing techniques to screen all GVA and GLRaVs strains in the samples.

4. Conclusion

Reliable detection of grapevine viruses in the field remains challenging due to varying symptomology. This study systematically compared the canopy growth response of SD-infected vines to healthy vines and proposed a rapid method to predict the SD infection in the Shiraz blocks using visible remote sensing technology. This technique has the potential to rapidly detect SD in the field, thereby providing prompt guidance for sampling locations for tissue testing of viruses as well as vineyard management. Further validation studies including various sites, seasons, cultivars, and virus strains are needed for this emerging technology. An additional, but important finding was that coinfection of GVA and GLRaVs results in significant vine devigoration in Shiraz, which does not occur with GVA or GLRaV alone. This observation was consistent across different soils and seasons under different weather conditions.

Data Availability

The raw and processed data used to support the study are available from the corresponding author upon request.

Conflicts of Interest

The authors declare that there are no conflicts of interest regarding publication of this work.

Acknowledgments

The authors gratefully acknowledged funding from South Australian Vine Improvement Association and Riverland Wine. We appreciate the top-up scholarship supported by Wine Australia. Special thanks to the industry collaborators: Kies Family Wines, and Mr Omer Najar from CCW Co-operative Limited.

References

[1] M. K. Corbett and J. Wiid, "Closterovirus-like particles in extracts from diseased grapevines," *Phytopathologia Mediterranea*, vol. 24, pp. 91–100, 1985.

[2] Q. Wu, N. Habili, F. Constable et al., "Virus pathogens in Australian vineyards with an emphasis on Shiraz Disease," *Viruses*, vol. 12, no. 8, p. 818, 2020.

[3] D. E. Goszczynski, "Single-strand conformation polymorphism (SSCP), cloning and sequencing reveal a close association between related molecular variants of Grapevine virus A (GVA) and Shiraz disease in South Africa," *Plant Pathology*, vol. 56, no. 5, pp. 755–762, 2007.

[4] N. Habili, "Australian shiraz disease: an emerging virus disease of *Vitis vinifera* cv. Shiraz," *Wine and Viticulture Journal*, vol. 28, no. 1, pp. 59–61, 2013.

[5] J. Charles, K. Froud, R. Van Den Brink, and D. Allan, "Mealybugs and the spread of grapevine leafroll-associated virus 3 (GLRaV-3) in a New Zealand vineyard," *Australasian Plant Pathology*, vol. 38, no. 6, pp. 576–583, 2009.

[6] G. Hommay, V. Komar, O. Lemaire, and E. Herrbach, "Grapevine virus A transmission by larvae of *Parthenolecanium corni*," *European Journal of Plant Pathology*, vol. 121, no. 2, pp. 185–188, 2008.

[7] D. E. Goszczynski and A. E. C. Jooste, "Identification of divergent variants of Grapevine virus A," *European Journal of Plant Pathology*, vol. 109, no. 4, pp. 397–403, 2003.

[8] D. E. Goszczynski and N. Habili, "Grapevine virus A variants of group II associated with Shiraz disease in South Africa are present in plants affected by Australian Shiraz disease, and have also been detected in the USA," *Plant Pathology*, vol. 61, no. 1, pp. 205–214, 2012.

[9] S. Chevalier, C. Greif, and P. Bass, B. Walter, Investigation on the aetiology of kober stem grooving disease," in *Proceedings of the 11th Meeting ICVG*, Montreux, Switzerland, September, 1993.

[10] R. Credi, "Characterization of grapevine rugose wood disease sources from Italy," *Plant Disease*, vol. 81, no. 11, pp. 1288–1292, 1997.

[11] M. Digiaro, M. P. Bedzrob, A. M. D'Onghia, D. Boscia, and V. N. Savino, "On the correlation between grapevine virus A and rugose wood," *Phytopathologia Mediterranea*, vol. 33, pp. 187–193, 1994.

[12] G. K. Blaisdell, S. Zhang, A. Rowhani et al., "Trends in vector-borne transmission efficiency from coinfected hosts: grapevine leafroll-associated virus-3 and Grapevine virus A," *European Journal of Plant Pathology*, vol. 156, no. 4, pp. 1163–1167, 2020.

[13] R. Naidu, A. Rowhani, M. Fuchs, D. Golino, and G. P. Martelli, "Grapevine leafroll: a complex viral disease affecting a high-value fruit crop," *Plant Disease*, vol. 98, no. 9, pp. 1172–1185, 2014.

[14] N. Habili, Q. Wu, and V. Pagay, "Virus-associated Shiraz Disease may lead Shiraz to become an endangered variety in Australia," *Wine and Viticulture Journal*, vol. 31, pp. 47–50, 2016.

[15] R. Almeida, K. Daane, V. Bell et al., "Ecology and management of grapevine leafroll disease," *Frontiers in Microbiology*, vol. 4, pp. 94–13, 2013.

[16] K. D. Ricketts, M. I. Gomez, S. S. Atallah et al., "Reducing the economic impact of Grapevine leafroll disease in California: identifying optimal disease management strategies," *American Journal of Enology and Viticulture*, vol. 66, no. 2, pp. 138–147, 2015.

[17] A. V. Zherdev, S. V. Vinogradova, N. A. Byzova, E. V. Porotikova, A. M. Kamionskaya, and B. B. Dzantiev, "Methods for the diagnosis of grapevine viral infections: a review," *Agriculture*, vol. 8, no. 12, p. 195, 2018.

[18] E. Rubinson, N. Galiakparov, S. Radian, I. Sela, E. Tanne, and R. Gafny, "Serological detection of grapevine virus A using antiserum to a nonstructural protein, the putative movement protein," *Phytopathology*, vol. 87, no. 10, pp. 1041–1045, 1997.

[19] R. R. Martin, K. C. Eastwell, A. Wagner, S. Lamprecht, and I. E. Tzanetakis, "Survey for viruses of grapevine in Oregon and Washington," *Plant Disease*, vol. 89, no. 7, pp. 763–766, 2005.

[20] Affinitylabs, "Virus testing [Online]," 2022, https://affinitylabs.com.au/virus-testing/.

[21] J. Albetis, S. Duthoit, F. Guttler et al., "Detection of Flavescence dorée Grapevine Disease using unmanned aerial

vehicle (UAV) multispectral imagery," *Remote Sensing*, vol. 9, no. 4, pp. 308–328, 2017.

[22] F. Vanegas, D. Bratanov, K. Powell, J. Weiss, and F. Gonzalez, "A novel methodology for improving plant pest surveillance in vineyards and crops using UAV-based hyperspectral and spatial data," *Sensors*, vol. 18, no. 1, p. 260, 2018.

[23] J. Ouyang, R. De Bei, and C. Collins, "Assessment of canopy size using UAV-based point cloud analysis to detect the severity and spatial distribution of canopy decline," *OENO One*, vol. 55, no. 1, 2021.

[24] S. L. Macdonald, M. Staid, M. Staid, and M. L. Cooper, "Remote hyperspectral imaging of grapevine leafroll-associated virus 3 in Cabernet Sauvignon vineyards," *Computers and Electronics in Agriculture*, vol. 130, pp. 109–117, 2016.

[25] S. Zia-Khan, M. Kleb, N. Merkt, S. Schock, and J. Müller, "Application of infrared imaging for early detection of Downy Mildew (*Plasmopara viticola*) in grapevine," *Agriculture*, vol. 12, no. 5, p. 617, Agriculture, 2022.

[26] Y. M. Wang, B. Ostendorf, D. Gautam, N. Habili, and V. Pagay, "Plant viral disease detection: from molecular diagnosis to optical sensing technology—a multidisciplinary review," *Remote Sensing*, vol. 14, no. 7, p. 1542, 2022.

[27] R. Raj, J. P. Walker, R. Pingale, R. Nandan, B. Naik, and A. Jagarlapudi, "Leaf area index estimation using top-of-canopy airborne RGB images," *International Journal of Applied Earth Observation and Geoinformation*, vol. 96, Article ID 102282, 2021.

[28] J. Monis and R. K. Bestwick, "Detection and localization of Grapevine Leafroll Associated Closteroviruses in greenhouse and tissue culture grown plants," *American Journal of Enology and Viticulture*, vol. 47, no. 2, pp. 199–205, 1996.

[29] E. Engvall and P. Perlmann, "Enzyme-linked immunosorbent assay, elisa," *The Journal of Immunology*, vol. 109, no. 1, pp. 129–135, 1972.

[30] G. Gambino, "Multiplex RT-PCR method for the simultaneous detection of nine grapevine viruses," *Methods in Molecular Biology*, vol. 1236, pp. 39–47, 2015.

[31] F. E. Constable and B. C. Rodoni, *Grapevine Leafroll-Associated Viruses*, Wine Australia, Adelaide, Australia, 2014.

[32] L. Breiman, "Random forests," *Machine Learning*, vol. 45, no. 1, pp. 5–32, 2001.

[33] D. E. Goszczynski, J. Du Preez, and J. T. Burger, "Molecular divergence of Grapevine virus A (GVA) variants associated with Shiraz disease in South Africa," *Virus Research*, vol. 138, no. 1-2, pp. 105–110, 2008.

[34] F. Fontaine, D. Gramaje, J. Armengol et al., *Grapevine Trunk Diseases. A Review*, OIV Publications, Paris, france, 2016.

[35] C. Bertsch, M. Ramírez-Suero, M. Magnin-Robert et al., "Grapevine trunk diseases: complex and still poorly understood," *Plant Pathology*, vol. 62, no. 2, pp. 243–265, 2013.

[36] D. Gramaje, J. R. Úrbez-Torres, and M. R. Sosnowski, "Managing grapevine trunk diseases with respect to etiology and epidemiology: current strategies and future prospects," *Plant Disease*, vol. 102, no. 1, pp. 12–39, 2018.

[37] G. P. Martelli, "Grapevine virology highlights 2006–2009," in *Proceedings of the 16th Meeting of the International Council for the Study of Virus and Virus-like Diseases of the Grapevine*, Dijon, France, September, 2009.